Title: State-dependent egocentric and allocentric heading representation in the monarch butterfly brain

Authors: M. Jerome Beetz[1]*, Christian Kraus[1], Myriam Franzke[1], David Dreyer[2], Martin F. Strube-Bloss[3], Wolfgang Rössler[1], Eric J. Warrant[2], Christine Merlin[4], Basil el Jundi[1]*

Affiliations:

[1]Zoology II, Biocenter, University of Würzburg, Würzburg, Germany

[2]Lund Vision Group, Department of Biology, Lund University, Lund, Sweden

[3]Department of Biological Cybernetics, University of Bielefeld, Bielefeld, Germany

[4]Department of Biology and Center for Biological Clocks Research, Texas A&M, College Station, TX, USA

*Corresponding authors

Email:

M. Jerome Beetz: jerome.beetz@uni-wuerzburg.de

Basil el Jundi: basil-el-jundi@uni-wuerzburg.de

Abstract: Head direction can be represented in a self-centered egocentric or a viewpoint-invariant allocentric reference frame. Using the most efficient representation is especially crucial for migrating animals, like monarch butterflies (*Danaus plexippus*) that use the sun for orientation. With tetrode recordings from the brain of tethered flying monarch butterflies, we examined the reference frame in which insects encode heading. We show that compass neurons switch their reference frame in a state-dependent manner. In quiescence, they encode sun-bearing angles, allowing the butterfly to map the environment within an egocentric frame. However, during flight, the same neurons encode heading within an allocentric frame. This switch converts the sun from a local to a global cue, an ideal strategy for maintaining a migratory heading over large distance.

One-Sentence Summary: Heading information is encoded in different state-dependent reference frames in the monarch butterfly central complex

Main Text: Goal-directed navigation requires animals to constantly register their heading in space. This is particularly important during long-distance migration, as exhibited by many vertebrates, such as birds and bats (*1*). Similarly, monarch butterflies annually migrate over 4,000 kilometers from southern Canada and the northern United States to their overwintering habitat in central Mexico (*2, 3*). To maintain their migratory heading, they use the sun as a global orientation reference (*4, 5*), which is processed in a brain region, the central complex (*6, 7*). There, sun compass neurons are expected to encode the butterflies' heading, like head-direction cells in vertebrates (*8-12*). Data from the central complex of *Drosophila* reveal that heading is encoded by a neural network composed of E-PG cells (*13-15*). These cells integrate visual input from ring neurons (*13, 16*) with wind input (*17*) and input from idiothetic, self-motion signals (*15, 18, 19*). Due to this multimodal nature, we hypothesize that the butterfly's heading-direction network strongly depends on the animal's locomotion state. However, due to methodological limitations, heading-direction cells have exclusively been recorded in restrained butterflies (*6*). Therefore, we designed an indoor flight arena that allowed us to perform tetrode recordings from tethered flying or quiescent butterflies (Fig. 1A). The upper inner circumference of the arena was equipped with a strip of individually switchable green light spots that served as sun stimuli that butterflies could use as an orientation reference for flight. During neural recordings from the central complex (Fig. 1B, S1) of tethered butterflies centered in the arena, an optical encoder measured the animal's heading direction. First, we recorded from quiescent butterflies resting on a platform at a fixed heading (0°; *quiescent pre-flight*; movie S1) while moving the light spot along a 360° circular path around the animal. To investigate the effect of flight activity on the neural response, we presented the same sun stimulus, but now with the same butterfly flying at a fixed heading (0°; *fixed flight*; movie S2). A subset of central-complex neurons (66 of 150 recorded neurons; 44%) exhibited state-dependent tuning to the solar azimuth. During *fixed flight*, 50 neurons (33%; 8 + 29 + 13 neurons outside the gray area in Fig. 1C) encoded the solar azimuth – indicated by an increase in firing rate at neuron-specific azimuthal positions of the sun stimulus – but showed no angular tuning during quiescence (Fig. 1D, green neuron). Conversely, 16 neurons (11%, 2+14 neurons of gray area in Fig. 1C) encoded the solar azimuth during quiescence but ceased to encode it during *fixed flight* (Fig. 1D, blue neuron). The remaining 84 of the 150 recorded neurons (56%) did not change their angular sensitivity to the sun stimulus in a state-dependent manner: 76 neurons were sensitive (51%; 56 + 20 neurons in merged gray and blue areas of Fig. 1C; example neuron in fig. S2A) and 8 neurons insensitive (5%; green area in Fig. 1C) during both states. Overall, the neurons showed broader tunings during flight than in quiescence (Wilcoxon signed rank test: $p < 0.0001$; fig. S3). To exclude the possibility that changes in angular sensitivity were due to unstable recording qualities, induced by movements during flight, we allowed the butterfly to settle on the platform after flight, and retested the neural sensitivity in 63 neurons (*quiescent post-flight*). All 63 neurons retained their *quiescent pre-flight* angular sensitivity (Fig. 1D, left versus right columns), suggesting that angular sensitivity depended on the animal's locomotory state. We also ruled out the possibility that we recorded from different neurons across the behavioral states by assessing the spike-shape stability through correlating averaged spike shapes within and across neurons (Fig. 1E, S2B, cf. Materials and Methods). For all neurons in the present study, the spike shapes within individual neurons statistically correlated better than with spike shapes across neurons suggesting that we recorded from the same neurons throughout the entire experiment.

Next, we examined the angular tuning while the butterflies were free to steer during flight i.e., rotate around their yaw axis while the sun stimulus was set at 0° (*steering flight*; movie S3). We classified 70 of the 150 recorded neurons as encoding the solar azimuth during *quiescence* and *steering flight* (Fig. 1F and G; 47% of the units; 14 + 56 neurons of gray portion in Fig. 1C).

Surprisingly, many of these neurons shifted their preferred firing direction to a different azimuthal position (Fig. 1F, blue neuron; fig. S4). These shifts mainly occurred during *steering flight*, which is indicated by dramatic changes in the neural response across a population of 27 neurons that were sensitive at each behavioral state (Fig. 1H). Moreover, the shifts were arbitrary across neurons indicated by a uniform distribution (Fig. 1J; Rayleigh test: $p = 0.09$, $n = 70$). In contrast, shifts in neural tuning rarely occurred between *quiescence* and *fixed flight*, and *quiescence pre-* and *post-flight* (Fig. 1I and 1K; respectively, $n = 76$ and 46 for *quiescent* versus *fixed flight* and *quiescent pre-* versus *quiescent post-flight*; V-test: $p < 0.0001$). Differences in the spatiotemporal dynamics of the sun stimulus i.e., history and velocity, could not explain the shifts in neural tuning measured during steering flights because the preferred firing directions did not change when the sun stimulus was unpredictably moved at different directions and velocities (movies S4 and S5; fig. S5A-S5C; $n = 42$ neurons; V-tests: $p < 0.001$). Thus, as with changes in the angular sensitivity, shifts in the preferred firing directions depended on the butterfly's behavioral state.

Next, we sought to examine the biological role of state-dependent changes in the sun compass. During *quiescence*, the neurons predominantly encoded the butterfly's frontal visual field ($n_{quiescent} = 92$ neurons; Figs. 2A; V-test: $p < 0.001$; fig. S6), whereas all compass directions were uniformly represented during *steering flight* ($n= 107$; Fig. 2B; Rayleigh test: $p = 0.83$). This indicates that the central complex changed its reference frame with the behavioral state: the neurons might encode the animal's bearing relative to the sun in quiescence (egocentric reference frame) and switch to a compass coding during *steering flight* (allocentric reference frame; Fig. 2C). To test this, we measured the central-complex activity (Fig. 2D) to an ambiguous visual stimulus, represented by two suns set 180° apart, while the butterflies were either quiescent or flying. As expected for an egocentric coding, the neurons showed a bimodal response when the two suns were rotated by 360° around a quiescent butterfly (left subpanels in Fig. 2E-F; *quiescent pre-flight*). Surprisingly, during flight the same neurons exhibited a unimodal response (middle subpanels in fig. 2E-F, *steering flight*) suggesting allocentric coding of heading directions. This is in line with studies in *Drosophila* moving in complex visual scenes, where heading is encoded by a single activity bump in the E-PG network (*13, 15, 20, 21*). Importantly, the neural coding returned to a bimodal response (i.e., egocentric coding) as soon as the animal settled (*quiescent post-flight*; right subpanels in Fig. 2E and 2F). The transition from an egocentric coding during quiescence to an allocentric coding during flight was highly significant (Fig. 2G; RM one-way ANOVA + Holm Sidák's multiple comparison test: $p < 0.001$, $n = 33$ neurons). These results clearly show that the changes in preferred firing directions observed during steering flights are a consequence of a state-dependent switch of the reference frame in which the central complex processes heading information.

What exactly triggers the switch to an allocentric coding during flight? One important aspect seems to be the change in angular sensitivity observed at flight onset (*fixed flights*, Fig. 1D). Although the firing rate of many neurons changed in a state-dependent manner (Fig. 1D, green neuron), it did not correlate with changes in angular sensitivity (fig. S7), which stands in contrast to findings from visual neurons in fruit flies (*22, 23*). One possible mechanism for the state-dependent change in angular sensitivity could be the modulation of the neurons' gain through the release of the neuromodulator octopamine, the invertebrate analog of noradrenaline (*24*). In the blowfly, a flight-induced increase of the octopamine level was correlated with changes in optic-flow processing (*25*). To test for octopaminergic effects in the monarch butterfly sun compass, we topically applied chlordimeform (CDM), an octopamine agonist that has commonly been used to mimic physiological effects associated with flight behavior (*25, 26*) onto the brain of quiescent butterflies ($N = 13$ animals; $n = 51$ neurons). Following CDM application, eight neurons (15 %,

Fig. 3, cyan neuron) became sensitive to sun stimulus position, whereas 16 neurons (31 %, Fig. 3, magenta neuron) lost this sensitivity. The remaining 26 neurons (51 %) maintained their previous angular sensitivities during CDM treatment. Octopaminergic modulation of neural sensitivity has been reported in optic lobe neurons in *Drosophila* (*27*) but so far such modulations have not been reported in brain centers downstream of the optic lobes, like the central complex. Since the total duration of CDM treatment was difficult to control, we electrically stimulated the central complex in quiescent butterflies in another set of experiments (20-40Hz, 2-4% duty cycle, 0.5-5 µA). Effects of electrical stimulation were similar to those from CDM treatment (fig. S8), but additionally it demonstrates the reversibility of these effects, with angular sensitivity being restored to pre-stimulation values, similar to our state-dependent findings (Fig. 1D). In the central complex of *Drosophila*, ring neurons providing visual input into the heading-direction network change their sensitivity in a state-dependent manner (*13, 16*), making these cells possible candidates for the state-dependent changes in angular sensitivity reported here. Although, we could mimic flight induced effects in angular sensitivity, CDM and electrical stimulations did not shift the preferred firing directions as observed during the switch in reference frames (Fig. 2). However, by modulating the visual input from the population of ring neurons in a state- and/or experience-dependent manner, the head-direction network of monarch butterflies gains flexibility (*13, 20*) that may be crucial for switches in reference frames in the central complex.

Many central-complex neurons encode turning behavior (*18, 19, 28*) which could induce the transition to an allocentric coding during the butterfly's *steering flight*. However, only 7 of the 150 recorded neurons conjunctively encoded flight turns and heading (5%; example neuron in fig. S5D-S5E). This indicates that we most likely did not record from the velocity input network (*18, 19*) or from output neurons (*29*) because these cell types encode turns in *Drosophila*. Thus, E-PG cells, termed CL1 cells in monarch butterflies (*7*), appear the most plausible candidate neurons in which switches of reference frames may occur.

The switch in the reference frame may be triggered by idiothetic signals that animals can use to infer their heading directions (*10, 12, 30*). As the central-complex neurons did not change their preferred firing direction when the animal was engaged in flight activity (*fixed flight*, Fig. 1), proprioceptive information from the wing muscles alone does not transform the compass to an allocentric representation. Two additional idiothetic inputs are reafference (e.g., motor efference copies) and vestibular-like signals that can compute the insect's heading even in darkness (*15, 31*). To test the relevance of vestibular-like inputs for the coding of heading information, we mounted the butterflies on a rotation stage in the arena's center. This allowed us to passively rotate the butterflies by 360° in the presence of a static sun stimulus (*quiescent rotation*; Fig. 4A and movie S6) followed by a rotation in darkness (*darkness rotation*). Similar to results in cockroaches (*31*) and rodents (*32, 33*), the preferred firing directions of the butterfly cells were invariant to the presence of visual stimuli (Fig. 4B-4E; n = 16 neurons; V-test: $p < 0.0001$). The persistence of neural tuning in darkness shows the involvement of mnemonic components and that the neurons represented heading directions – rather than purely processing visual information – in quiescence. The tuning during *darkness rotation* was significantly broader than during *quiescent rotation* (Wilcoxon signed rank test: $p = 0.0076$; fig. S9) which makes sense because computing heading directions with idiothetic cues only accumulates errors over time (*10*). The preferred firing directions measured in the presence of vestibular-like signals (*quiescent rotation*) were almost identical to the ones measured in the absence of vestibular-like signals (*quiescent*; Fig. 4D and 4F; n = 16 neurons; V-test: $p < 0.0001$). Vestibular-like signals alone did not induce an allocentric compass coding as observed in the same neurons during *steering flight* (Fig. 4D and 4G; n = 16 neurons; Rayleigh test: $p = 0.6$). Alternatively, reafference signals arising from steering commands

might be the trigger to switch to an allocentric representation. To verify this, we set visual and idiothetic cues in conflict by abruptly displacing the solar azimuth by 180° relative to the animal and measuring neural tuning in the absence (*quiescent* butterflies being rotated) or in the presence of reafference signals (tethered butterflies performing *steering flights)*. In the absence of reafference signals, the heading coding was anchored to the sun stimulus and the neurons changed their neural tuning by about 180° which further supports the interpretation of an egocentric coding (Fig. 4H and 4I; n = 37 neurons; V-test: $p < 0.001$). Interestingly, in the presence of reafference signals, the neurons retained their neural tuning after sun stimulus displacement as expected from an allocentric coding (Fig. 4J and 4K; n = 22 neurons; V-test: $p = 0.02$). To further demonstrate the influence of reafference signals on the switch to an allocentric representation, we tethered the butterflies dorsally to a rotation stage that allowed us to passively change their heading during fixed flights (*rotation fixed flight*; movie S7). Even when the butterflies performed fixed flights – in the presence of vestibular-like and proprioceptive signals but in the absence of reafference signals – the heading-direction was egocentrically represented indicated by no change in the neural tuning (fig. S10; n = 17 neurons; V-test: $p< 0.001$). Together, our results suggest that reafferent signals arising from active steering represent the most likely source that transforms the monarch butterfly heading-direction network into an allocentric frame of reference. While previous studies reported state-dependent changes of the sensitivity of central-complex neurons (*34, 35*), the functional implication of these changes have remained unclear. We here show for the first time in insects that active orientation has a dramatic impact on the processing of heading direction information in the brain, as shown for mammals (*32, 36*). Through active orientation, the central-complex network switches its reference frame to employ the most efficient strategy to represent the animal's surroundings. In quiescent animals, the heading-direction network operates in an egocentric reference frame when local cues in the vicinity of the butterfly are ethologically most relevant. In contrast, global information dominates when the animal rapidly moves through space which results in an allocentric coding of heading-directions. Although transitions between reference frames have been extensively studied in mammals (*37, 38*), the neural mechanisms underlying such transitions in invertebrates have remained enigmatic. The transition of the heading-direction network into an allocentric compass during flight requires the integration of idiothetic cues, including reafferent and proprioceptive signals, and allothetic cues, including the sun (*4, 39, 40*) and/or the earth's magnetic field (*41, 42*) to allow monarch butterflies to efficiently maintain their migratory direction during their long journey.

References and Notes:

1. H. Mouritsen, Long-distance navigation and magnetoreception in migratory animals. *Nature* **558**, 50-59 (2018).
2. S. M. Reppert, R. J. Gegear, C. Merlin, Navigational mechanisms of migrating monarch butterflies. *Trends Neurosci* **33**, 399-406 (2010).
3. S. M. Reppert, P. A. Guerra, C. Merlin, Neurobiology of Monarch Butterfly Migration. *Annu Rev Entomol* **61**, 25-42 (2016).
4. H. Mouritsen, B. J. Frost, Virtual migration in tethered flying monarch butterflies reveals their orientation mechanisms. *Proc Natl Acad Sci U S A* **99**, 10162-10166 (2002).
5. S. M. Perez, O. R. Taylor, R. Jander, A Sun compass in monarch butterflies. *Nature* **387**, 29-29 (1997).
6. S. Heinze, S. M. Reppert, Sun Compass Integration of Skylight Cues in Migratory Monarch Butterflies. *Neuron* **69**, 345-358 (2011).

7. S. Heinze, J. Florman, S. Asokaraj, B. El Jundi, S. M. Reppert, Anatomical basis of sun compass navigation II: the neuronal composition of the central complex of the monarch butterfly. *J Comp Neurol* **521**, 267-298 (2013).
8. A. Finkelstein *et al.*, Three-dimensional head-direction coding in the bat brain. *Nature* **517**, 159-164 (2015).
9. E. Vinepinsky *et al.*, Representation of edges, head direction, and swimming kinematics in the brain of freely-navigating fish. *Sci Rep* **10**, 14762 (2020).
10. J. S. Taube, The head direction signal: origins and sensory-motor integration. *Annu Rev Neurosci* **30**, 181-207 (2007).
11. J. S. Taube, R. U. Muller, J. B. Ranck, Jr., Head-direction cells recorded from the postsubiculum in freely moving rats. I. Description and quantitative analysis. *J Neurosci* **10**, 420-435 (1990).
12. K. E. Cullen, J. S. Taube, Our sense of direction: progress, controversies and challenges. *Nat Neurosci* **20**, 1465-1473 (2017).
13. Y. E. Fisher, J. Lu, I. D'Alessandro, R. I. Wilson, Sensorimotor experience remaps visual input to a heading-direction network. *Nature* **576**, 121-125 (2019).
14. S. S. Kim, H. Rouault, S. Druckmann, V. Jayaraman, Ring attractor dynamics in the Drosophila central brain. *Science* **356**, 849-U111 (2017).
15. J. D. Seelig, V. Jayaraman, Neural dynamics for landmark orientation and angular path integration. *Nature* **521**, 186-+ (2015).
16. J. D. Seelig, V. Jayaraman, Feature detection and orientation tuning in the Drosophila central complex. *Nature* **503**, 262-266 (2013).
17. T. S. Okubo, P. Patella, I. D'Alessandro, R. I. Wilson, A Neural Network for Wind-Guided Compass Navigation. *Neuron* **107**, 924-940 e918 (2020).
18. D. Turner-Evans *et al.*, Angular velocity integration in a fly heading circuit. *Elife* **6**, (2017).
19. J. Green *et al.*, A neural circuit architecture for angular integration in Drosophila. *Nature* **546**, 101-+ (2017).
20. S. S. Kim, A. M. Hermundstad, S. Romani, L. F. Abbott, V. Jayaraman, Generation of stable heading representations in diverse visual scenes. *Nature* **576**, 126-131 (2019).
21. Y. M. Giraldo *et al.*, Sun Navigation Requires Compass Neurons in Drosophila. *Curr Biol* **28**, 2845-2852 e2844 (2018).
22. G. Maimon, A. D. Straw, M. H. Dickinson, Active flight increases the gain of visual motion processing in Drosophila. *Nature Neuroscience* **13**, 393-U329 (2010).
23. M. E. Chiappe, J. D. Seelig, M. B. Reiser, V. Jayaraman, Walking Modulates Speed Sensitivity in Drosophila Motion Vision. *Current Biology* **20**, 1470-1475 (2010).
24. I. Orchard, J. M. Ramirez, A. B. Lange, A Multifunctional Role for Octopamine in Locust Flight. *Annual Review of Entomology* **38**, 227-249 (1993).
25. K. D. Longden, H. G. Krapp, State-Dependent Performance of Optic-Flow Processing Interneurons. *J Neurophysiol* **102**, 3606-3618 (2009).
26. S. N. Jung, A. Borst, J. Haag, Flight activity alters velocity tuning of fly motion-sensitive neurons. *J Neurosci* **31**, 9231-9237 (2011).
27. M. P. Suver, A. Mamiya, M. H. Dickinson, Octopamine Neurons Mediate Flight-Induced Modulation of Visual Processing in Drosophila. *Current Biology* **22**, 2294-2302 (2012).
28. J. P. Martin, P. Y. Guo, L. Y. Mu, C. M. Harley, R. E. Ritzmann, Central-Complex Control of Movement in the Freely Walking Cockroach. *Current Biology* **25**, 2795-2803 (2015).

29. H. M. Shiozaki, K. Ohta, H. Kazama, A Multi-regional Network Encoding Heading and Steering Maneuvers in Drosophila. *Neuron* **106**, 126-+ (2020).
30. A. G. Varga, N. D. Kathman, J. P. Martin, P. Y. Guo, R. E. Ritzmann, Spatial Navigation and the Central Complex: Sensory Acquisition, Orientation, and Motor Control. *Front Behav Neurosci* **11**, (2017).
31. A. G. Varga, R. E. Ritzmann, Cellular Basis of Head Direction and Contextual Cues in the Insect Brain. *Curr Biol* **26**, 1816-1828 (2016).
32. M. E. Shinder, J. S. Taube, Self-motion improves head direction cell tuning. *J Neurophysiol* **111**, 2479-2492 (2014).
33. S. Coletta, M. Frey, K. Nasr, P. Preston-Ferrer, A. Burgalossi, Testing the Efficacy of Single-Cell Stimulation in Biasing Presubicular Head Direction Activity. *Journal of Neuroscience* **38**, 3287-3302 (2018).
34. J. A. Bender, A. J. Pollack, R. E. Ritzmann, Neural activity in the central complex of the insect brain is linked to locomotor changes. *Curr Biol* **20**, 921-926 (2010).
35. P. T. Weir, M. H. Dickinson, Functional divisions for visual processing in the central brain of flying Drosophila. *Proc Natl Acad Sci U S A* **112**, E5523-5532 (2015).
36. R. W. Stackman, E. J. Golob, J. P. Bassett, J. S. Taube, Passive transport disrupts directional path integration by rat head direction cells. *J Neurophysiol* **90**, 2862-2874 (2003).
37. A. Bicanski, N. Burgess, Neuronal vector coding in spatial cognition. *Nat Rev Neurosci* **21**, 453-470 (2020).
38. B. J. Clark, C. M. Simmons, L. E. Berkowitz, A. A. Wilber, The Retrosplenial-Parietal Network and Reference Frame Coordination for Spatial Navigation. *Behav Neurosci* **132**, 416-429 (2018).
39. I. Sauman *et al.*, Connecting the navigational clock to sun compass input in monarch butterfly brain. *Neuron* **46**, 457-467 (2005).
40. C. Merlin, R. J. Gegear, S. M. Reppert, Antennal Circadian Clocks Coordinate Sun Compass Orientation in Migratory Monarch Butterflies. *Science* **325**, 1700-1704 (2009).
41. G. Wan, A. N. Hayden, S. E. Iiams, C. Merlin, Cryptochrome 1 mediates light-dependent inclination magnetosensing in monarch butterflies. *Nat Commun* **12**, 771 (2021).
42. P. A. Guerra, R. J. Gegear, S. M. Reppert, A magnetic compass aids monarch butterfly migration. *Nat Commun* **5**, 4164 (2014).
43. M. Franzke *et al.*, Spatial orientation based on multiple visual cues in non-migratory monarch butterflies. *J Exp Biol* **223**, (2020).
44. B. el Jundi *et al.*, Neural coding underlying the cue preference for celestial orientation. *P Natl Acad Sci USA* **112**, 11395-11400 (2015).
45. W. Edrich, C. Neumeyer, O. V. Helversen, Anti-Sun Orientation of Bees with Regard to a Field of Ultraviolet-Light. *J Comp Physiol* **134**, 151-157 (1979).
46. S. Rossel, R. Wehner, Celestial Orientation in Bees - the Use of Spectral Cues. *J Comp Physiol* **155**, 605-613 (1984).
47. M. F. Strube-Bloss, M. P. Nawrot, R. Menzel, Mushroom body output neurons encode odor-reward associations. *J Neurosci* **31**, 3129-3140 (2011).
48. M. F. Brill, M. Reuter, W. Rossler, M. F. Strube-Bloss, Simultaneous long-term recordings at two neuronal processing stages in behaving honeybees. *J Vis Exp*, (2014).
49. M. F. Strube-Bloss, M. P. Nawrot, R. Menzel, Neural correlates of side-specific odour memory in mushroom body output neurons. *Proc Biol Sci* **283**, (2016).
50. T. A. T. Nguyen, M. J. Beetz, C. Merlin, B. El Jundi, Sun compass neurons are tuned to migratory orientation in monarch butterflies. *Proc Biol Sci* **288**, 20202988 (2021).

51. P. Berens, CircStat: A MATLAB Toolbox for Circular Statistics. *J Stat Softw* **31**, 1-21 (2009).
52. F. Zittrell, K. Pfeiffer, U. Homberg, Matched-filter coding of sky polarization results in an internal sun compass in the brain of the desert locust. *Proc Natl Acad Sci U S A* **117**, 25810-25817 (2020).

Acknowledgments: We thank Marie Dacke, Keram Pfeiffer, and Jan Ache for their helpful comments on our manuscript and Jan Ache for providing us with chlordimeform for pharmacological experiments. We thank Manu Madhav and Flavio Rocces for discussing our results. We thank Keram Pfeiffer and Konrad Öchsner for their help in setting up the LED stimulus and Fabian Schmalz for introducing Neuralynx and spike sorting in spike2. In addition, we thank Sergio Siles (butterflyfarm.co.cr) and Marie Gerlinde Blaese for providing us with monarch butterfly pupae.

Funding: This work was funded by the Emmy Noether program of the German Research Foundation granted to BeJ (Grant number: EL784/1-1) and a European Research Council Advanced Grant to EJW (MagneticMoth 741298).

Author contributions:

Conceptualization: MJB, BJ

Methodology: MJB, MSB, CK, MF, DD, WR

Formal Analysis; MJB, BJ

Investigation: MJB, CK

Visualization: MJB, CK, BJ

Funding acquisition: BJ, EJW

Project administration: BJ, WR, CM

Supervision: BJ

Writing – original draft: MJB, BJ

Writing – review & editing: MJB, CK, MF, DD, MSB, WR, EJW, CM, BJ

Competing interests: Authors declare that they have no competing interests.

Data and materials availability: Matlab files with the calculated response parameters of the neurons together with the Matlab-scripts used for the analysis and Arduino scripts used for stimulus presentation are accessible from the Figshare Repository: doi.org/10.6084/m9.figshare.14381375

Supplementary Materials

Materials and Methods

Figs. S1 to S10

References (*43–52*)

Movies S1 to S7

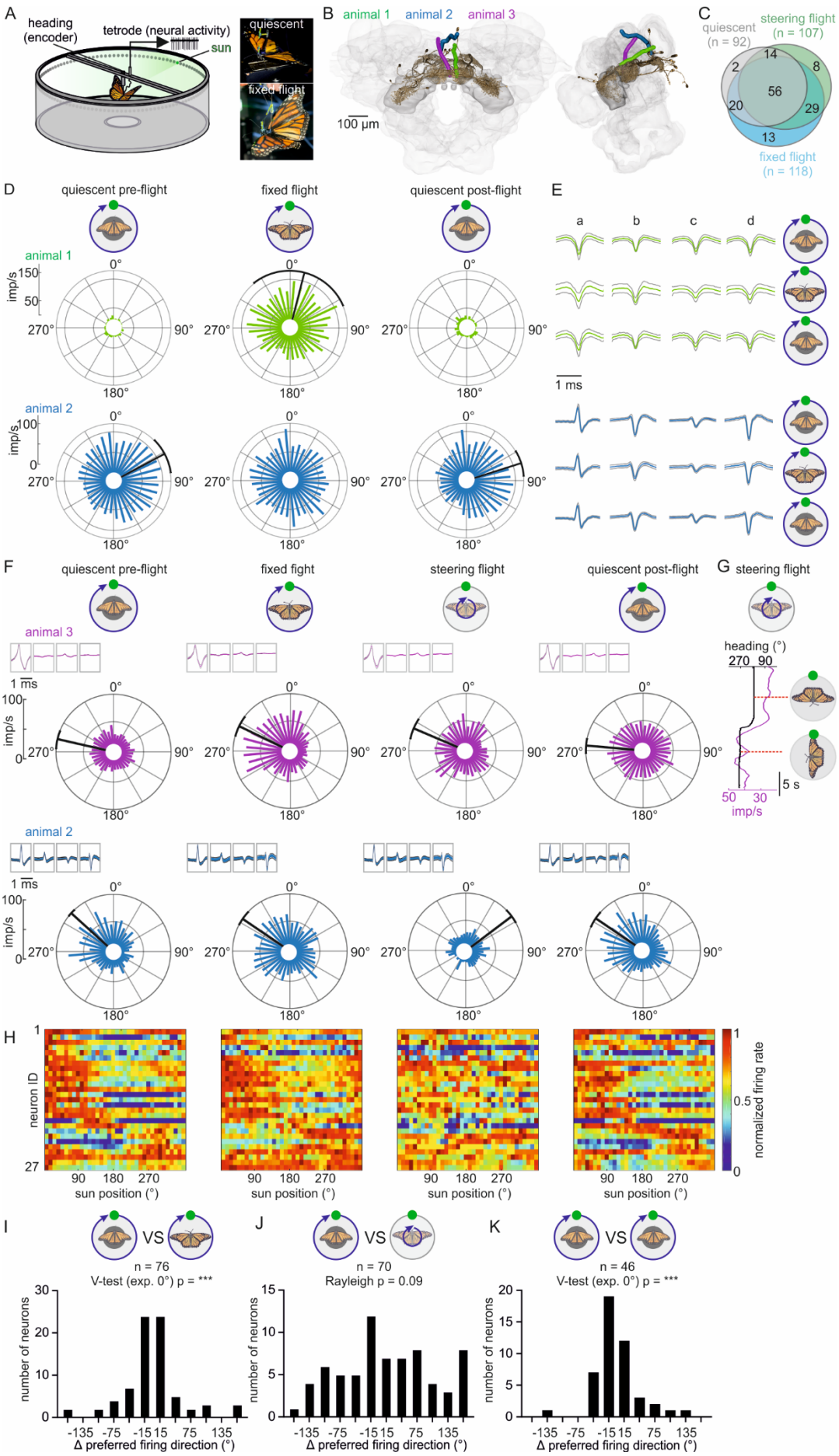
A
heading (encoder)
tetrode (neural activity)
sun
quiescent
fixed flight
B
animal 1
animal 2
animal 3
100 µm
C
quiescent (n = 92)
steering flight (n = 107)
fixed flight (n = 118)
14
2
8
56
20
29
13
D
quiescent pre-flight
fixed flight
quiescent post-flight
animal 1
animal 2
imp/s
E
a
b
c
d
1 ms
F
quiescent pre-flight
fixed fight
steering flight
quiescent post-flight
animal 3
animal 2
G
steering flight
heading (°)
270 90
5 s
50 30
imp/s
H
neuron ID
sun position (°)
normalized firing rate
I
n = 76
V-test (exp. 0°) p = ***
J
n = 70
Rayleigh p = 0.09
K
n = 46
V-test (exp. 0°) p = ***
number of neurons
Δ preferred firing direction (°)

Fig. 1. State-dependent changes of the monarch butterfly sun compass. (**A**) Schematic setup of a tethered butterfly in a flight arena. Heading direction was measured with an encoder while neural activity from the central complex was recorded with tetrodes. A green light spot served as a sun stimulus. (**B**) Reconstructed tetrode tracks (one from each animal, indicated in different colors) warped into the standardized monarch butterfly central complex (*7*). Prominent central-complex neurons (*7*) are visualized (*brown*). The brain is shown from an antero-dorsal (*left*) and a lateral (*right*) view. (**C**) Number of neurons encoding the solar azimuth across different behavioral states i.e., *quiescent, fixed flight, steering flight*. (**D**) Circular plots from two example neurons (*blue*, *green*) showing firing rate at different sun positions and at different behavioral states i.e., *quiescent pre-flight (left), fixed flight (middle), quiescent post-flight (right)*. The animal faced 0° while the sun stimulus moved around it. Black lines and sectors represent the preferred firing direction ± standard deviation (*SD*) of neurons that encoded the solar azimuth (Rayleigh test: $p < 0.05$). (**E**) Spike shapes (*mean* ± *IQR*) of individual tetrode channels (*a-d*) calculated for each behavioral state for the blue and green example neurons in (D). (**F**) The firing rates of two neurons (*magenta*, *blue*) in two individuals at different sun positions relative to the animal's heading (pointing towards 0°) for four behavioral states. The average spike shape recorded at each electrode is shown at the upper left corner for each behavioral state. (**G**) Section from a steering flight demonstrates the correlation between the animal's heading (*black*) and a neuron's firing rate (*magenta*). (**H**) Neural activity (color coded) of 27 neurons (*y-axis*) plotted against the sun position (*x-axis*) for each behavioral state. Only neurons that were sensitive (Rayleigh test: $p < 0.05$) across all four behavioral states are included. (**I-K**) Changes in preferred firing direction between *quiescent pre-flight* and *fixed flight* (I), *quiescent pre-flight* and *steering flight* (J), and *quiescent pre-flight* and *quiescent post-flight* (K).

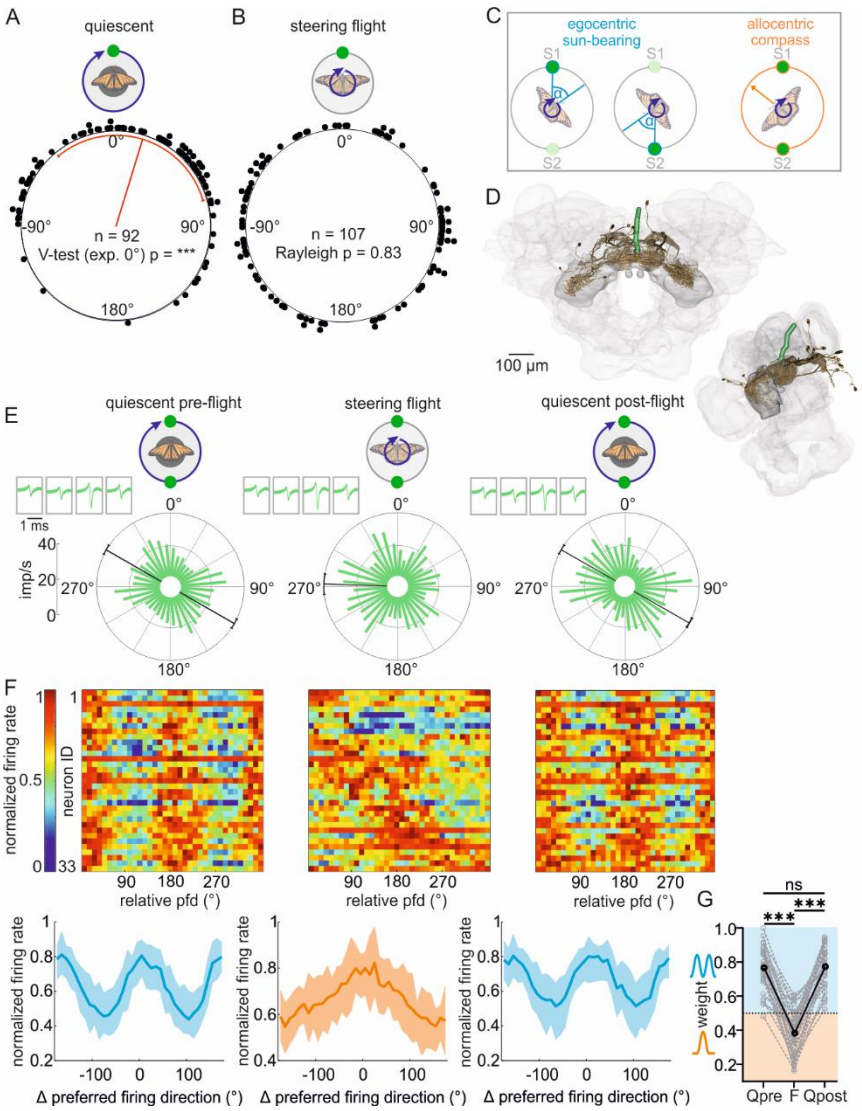

Fig. 2. Heading-direction network of monarch butterflies changes its reference frame from egocentric to allocentric coding during flight. (A-B) Distribution of the preferred firing directions during *quiescence* (A) and *steering flight* (B). (**C**) Schema of the reference frames (*blue* = egocentric sun-bearing; *orange* = allocentric heading-direction) when the butterflies orient in an ambiguous visual scene with two simulated suns set 180° apart (*S1* and *S2*). (**D**) Tetrode position from the neuron recorded in (E). The brain is shown from an antero-dorsal (*left*) and a lateral (*right*) view. (**E**) The response of a neuron when the butterfly was quiescent, and the ambiguous stimulus was rotated around the animal (*left* and *right*) and when the butterfly was flying while the ambiguous stimulus was stationary (*middle*). Average spike shapes are indicated at the top left corner. (**F**) (*Top*) Responses (*color coded*) of 33 neurons in each behavioral state. Along the x-axis, the heatmaps were aligned to the neuron's preferred firing direction (*pfd*) of the *quiescent pre-flight* condition to emphasize the bimodal response during quiescence. Along the y-axis, the neurons were ordered according to the pfd measured during steering flight. (*Bottom*) Averaged response (mean ± quantile) of all 33 neurons during quiescence (*left*, *right*) and during flight (when the neurons' maximum responses were shifted to 0°). (**G**) Weights of the neural responses of the 33 neurons to a bimodal or unimodal fit for each behavioral state i.e., *quiescent pre-flight (Q_{pre}), steering flight (F), quiescent post-flight (Q_{post})*. A weight between 0 and 0.5 indicates that the neural response was unimodal, whereas a weight between 0.5 and 1 indicates that the neural response was bimodal. Mean weights are indicated by black lines. ***: $p < 0.0001$; ns: $p > 0.05$; Friedman test.

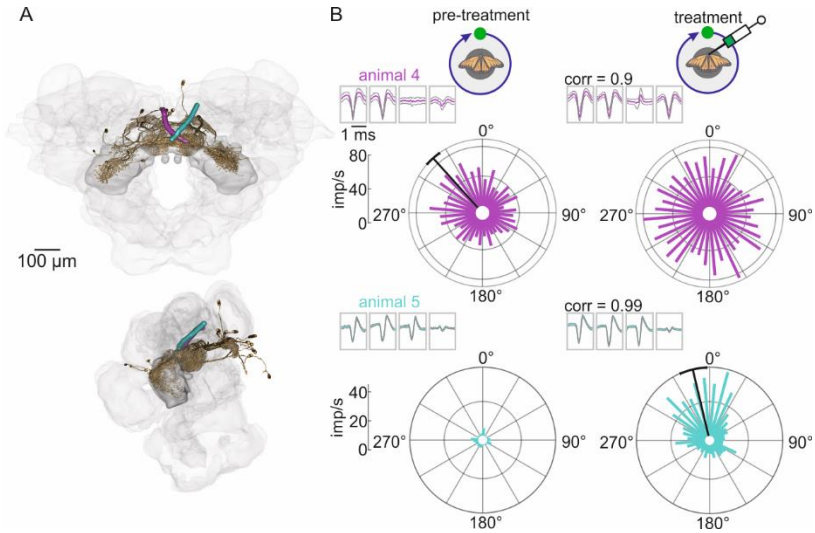

Fig. 3. Changes in neural sensitivity for encoding the solar azimuth could be mimicked by chlordimeform application. (**A**) Tetrode tracks (one from each animal, indicated in different colors) were reconstructed and warped into the standardized monarch butterfly central complex (*7*). Prominent central-complex neurons (*7*) are shown (*brown*). The brain is shown from an antero-dorsal (*left*) and a lateral (*right*) view. (**B**) Circular plots of two neurons in two individuals [corresponding to magenta and cyan electrode track in (A)] that changed their sensitivity after chlordimeform application in quiescent animals. Corresponding spike shapes (*mean* ± *IQR*) and correlation coefficients (*corr*) are indicated at the top left corner of each circular plot.

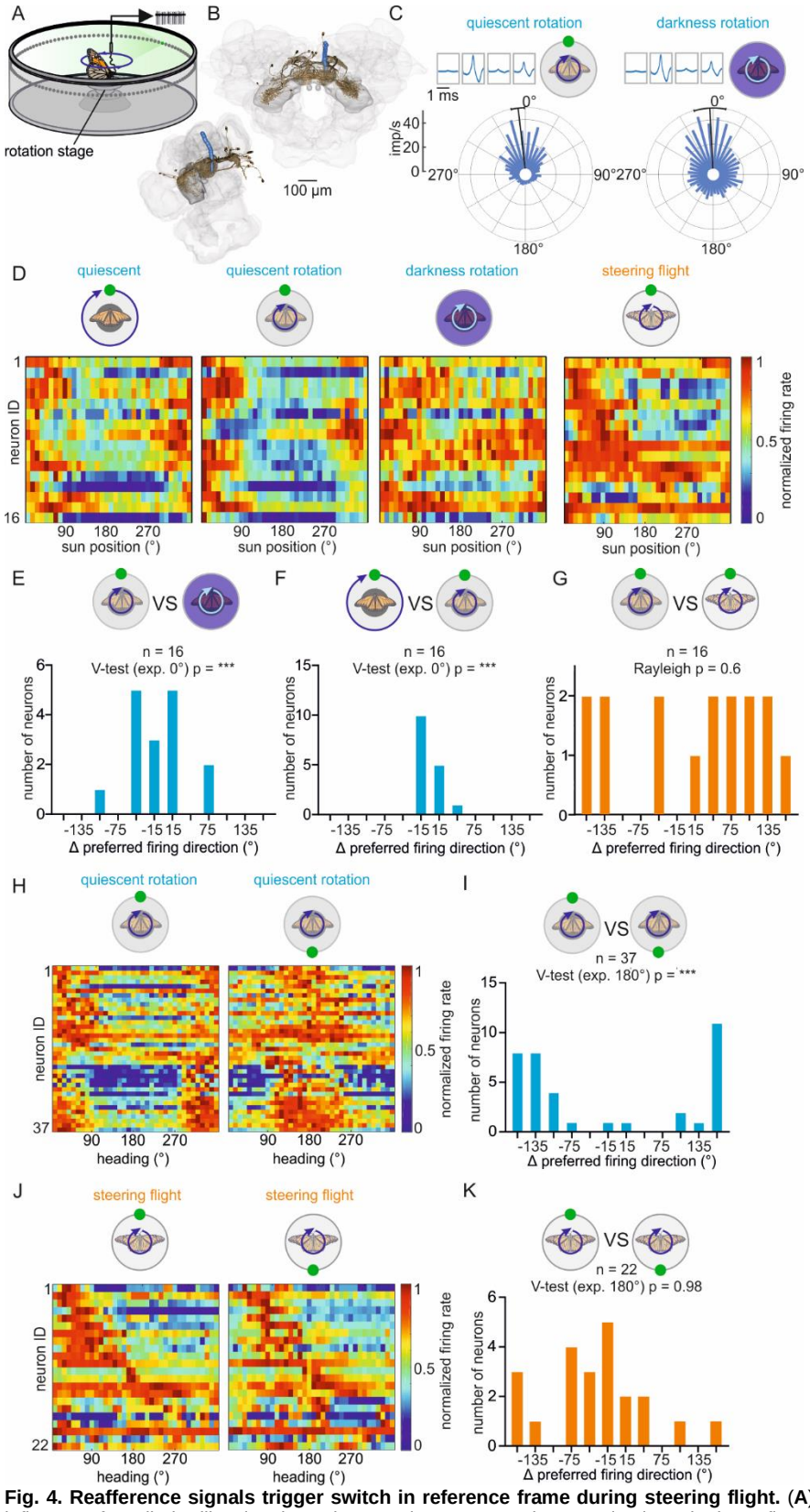

Fig. 4. Reafference signals trigger switch in reference frame during steering flight. (**A**) Illustration of the setup to test for the influence of vestibular-like signals on the neural response to the sun stimulus. The butterfly was mounted on a rotating platform while performing tetrode recordings from the central complex. (**B**) Tetrode position during the experiment in which the example neuron in (C) was recorded. The brain is shown from an antero-dorsal (*top*) and a lateral (*bottom*) view. (**C**) A neuron showing a preferred firing direction when the butterfly was rotated in the presence of the sun stimulus (*left*) and in darkness (*right*). Average spike shapes are indicated at the top. (**D**) Neural activity from 16 neurons in each behavioral state is plotted against the sun position. Only neurons that

were sensitive (Rayleigh test: $p < 0.05$) in all behavioral states were included. (**E-G**) Changes in the preferred firing direction during *quiescent rotation* and rotation in darkness (*darkness rotation*) (E), in the absence (*quiescent*) and in presence of vestibular-like input (*quiescent rotation*) (F), and *quiescent rotation* and *steering flight* (G). (**H**) The neural activity of 37 neurons plotted against the animal's heading when the sun stimulus was positioned at 0° (left) and 180° (right) and the animal was rotated by 360° around its body axis (*rotation*). (**I**) Changes in the preferred firing direction between the sun stimulus positioned at 0° and at 180° when the animal was rotated. Most neurons shifted their preferred firing directions by 180° (V-test: $p < 0.001$) which indicates egocentric sun-bearing coding during quiescence. (**J**) The neural activity of 22 neurons plotted against the animal's heading when the sun stimulus was positioned at 0° (*left*) or at 180° (*right*) while the animals were able to steer during flight. (**K**) The changes in preferred firing direction between the sun stimulus positioned at 0° and at 180°. The change of preferred firing direction was clustered around 0° (V-test: $p = 0.02$) which suggests an allocentric compass coding during flight.

Supplementary Materials for

State-dependent egocentric and allocentric heading representation in the monarch butterfly brain

M. Jerome Beetz*, Christian Kraus, Myriam Franzke, David Dreyer, Martin F. Strube-Bloss, Wolfgang Rössler, Eric J. Warrant, Christine Merlin, Basil el Jundi*

*Correspondence to: jerome.beetz@uni-wuerzburg.de; basil-el-jundi@uni-wuerzburg.de

This PDF file includes:

Materials and Methods
Figs. S1 to S10
Captions for Movies S1 to S7

Other Supplementary Materials for this manuscript include the following:

Movies S1 to S7

Materials and Methods

Animals

Monarch butterflies (*Danaus plexippus*) were ordered as pupae from Costa Rica Entomology Supply (butterflyfarm.co.cr) and kept in an incubator (HPP 110 and HPP 749, Memmert GmbH + Co. KG, Schwabach, Germany) at 25°C, 80% relative humidity and 12:12 light/dark-cycle conditions. After eclosion, the adult butterflies were transferred into a different incubator (I-30VL, Percival Scientific, Perry, IA, USA) at 25°C and 12:12 light/dark condition. Adults had access to 15% sucrose diluted in water *ad libitum*. In total, we tested 89 butterflies.

Setup for simultaneous behavioral and electrophysiological recordings

To record neural activity in the butterfly brain, signals from custom-built tetrodes (see Tetrodes and Implantation) were passed through an electrode interface board (EIB-18; Neuralynx Inc., Bozeman, MT, USA) and an adapter board (ADPT-DUAL-HS-DRS; Neuralynx Inc., Bozeman, MT, USA) to a Neuralynx recording system (DL 4SX 32ch System, Neuralynx Inc., Bozeman, MT, USA). The neural activity was monitored using the software Cheetah (Neuralynx Inc., Bozeman, MT, USA). During recording, the heading direction of a butterfly was observed in a flight arena similar to the ones described before (*4*, *43*). The arena had an inner diameter of 32 cm and a height of 12 cm (Fig. 1A). A tungsten rod was attached to the butterfly's thorax using a magnet (diameter = 3 mm; magnetic force = 4 N; Supermagnete, Webcraft GmbH, Gottmadingen, Germany) as well as dental wax (Article: 54895 Omnident, Rodgau Nieder-Roden, Germany) and was connected dorsally to an optical encoder (E4T miniature Optical Kit Encoder, US Digital, Vancouver, WA, USA) at the center of the arena. To avoid wrapping the tetrode wires around the tungsten rod, the animals' rotatory movements were restricted to 358°. The heading direction was measured at a sampling rate of 100 Hz and with an angular resolution of 3°. These measurements were then digitized (USB4 Encoder Data Acquisition USB Device, US Digital, Vancouver, WA, USA). The animal's heading was observed in the US Digital software (USB1, USB4: US Digital, Vancouver, WA, USA). A trigger signal at the onset of the behavioral recording was sent via an ATLAS analog isolator (Neuralynx Inc., Bozeman, MT, USA) and the adapter board to the Neuralynx recording system. This allowed us to align the behavioral data from the encoder with our neural recordings in the software Spike2 (version 9.0 Cambridge Electronic Devices, Cambridge, UK) after an experiment. The upper inner circumference of the flight arena was equipped with 144 RGB-LEDs (Adafruit NeoPixel, Adafruit Industries, New York, New York, USA) at an elevation of ~ 30° relative to the butterfly. One of these LEDs, when lit, provided a single green light spot as a stimulus (1.74×10^{13} photons/cm^2/s and 1.2° angular subtense, as measured at the center of the arena). Insects interpret such a stimulus as the sun (*44-46*). The angular position of the green light spot was controlled with an Arduino MEGA 2560. An analog output from the Arduino was sent via the ATLAS analog isolator to the Neuralynx recording system and allowed us to align the stimulus presentation with the neural activity.

Tetrodes and Implantation

To record neural activity in the butterfly brain central complex, we adopted and modified the recording method that has been successfully established in honeybees to record learning related plasticity (*47-49*). A tetrode was built by waxing five (four recording wires and one differential

wire) 18 cm long and 12.5 µm thin (10µm + insulation) copper wires (P155, Elektrisola, Reichshof-Eckenhagen, Germany) together. The tetrode was carefully threaded through two Pebax® tubes (each 2-4 cm in length; 0.026' inner diameter; Zeus Inc, Orangeburg, SC, USA) that served as attaching points to mount the tetrode to a glass capillary. Tetrode and glass capillary were then attached to an electrode holder (M3301EH; WPI, Sarasota, FL, USA). The tetrode wires were connected to different channels of the EIB-18. A separate wire was connected to the grounding pin of the EIB-18 and served as grounding wire. To reduce the resistance of each electrode to about 0.1-1 MΩ, the tips of the tetrode wires were plated with gold (Elektrolyt Gold solution, Conrad Electronic SE, Hirschau, Germany). The resistance of each tetrode wire was measured using a nanoZ (Multi Channel Systems MCS GmbH, Reutlingen, Germany). To position the tetrode in the butterfly brain, the electrode holder (together with the EIB-18 and the tetrode) was connected to a micromanipulator (Sensapex, Oulu, Finland). For tetrode implantation, a monarch butterfly was horizontally restrained on a magnetic holder. The head was waxed to the thorax to avoid head movements during recording and flight. The head capsule was opened dorsally and fat and trachea on top of the brain were removed. To gain access to the central complex, the neural sheath on the dorsal brain surface was carefully removed using fine tweezers. The grounding wire was placed posteriorly in the head capsule. To identify the tetrode position, the tip of the tetrode was immersed in ALEXA 647 Hydrazide (A20502, Thermo Fisher Scientific GmbH, Dreieich, Germany) or ALEXA 568 Hydrazide (A10437, Thermo Fisher Scientific GmbH, Dreieich, Germany) diluted in 0.5 M KCl. Tetrodes were then inserted into the central brain while measuring neural signals with a sampling frequency of 30 kHz and a band-pass filter (600-6000Hz). One of the five tetrode wires was selected as a reference in the recording software and its signal was subtracted from the signals of the remaining four tetrode wires to obtain a differential signal. After finding neurons encoding the angular position of the sun stimulus, the tetrode and the grounding wire were held in place by adding a two-component silicone elastomer (Kwik-Sil, WPI, Sarasota, FL, USA). After the Kwik-Sil hardened (~ 1 hour), the butterfly was carefully unrestrained and connected to the end of the tungsten rod that was connected to the optical encoder. The tetrodes were carefully removed from the glass capillary and attached to a Pebax® tube to the tungsten rod. This setup allowed us to obtain stable neural recordings for several hours and when the butterfly was either tethered flying or quiescent on a platform.

Visualization of electrode tracks

After neural recording, the brain was dissected out of the head and fixated overnight in 4% formaldehyde at 4°C. After fixation, the brain was transferred into sodium-phosphate buffer (NaPi) and rinsed for 2 x 20 and 3 x 20 minutes in 0.1 M phosphate buffered saline (PBS) and PBS with 0.3% Triton-X (PBT), respectively. The brain was dehydrated with an ascending ethanol series (30% - 100%, 15 minutes each) and immersed with a 1:1 ethanol-methyl-salicylate solution for 15 minutes, followed by a clearing step in methyl-salicylate for at least 1 hour. The brain was embedded in Permount (Fisher Scientific GmbH, Schwerte, Germany) between two cover slips and scanned with a confocal microscope (Leica TCS SP2, Wetzlar, Germany) using a 10x water immersion objective (HCX PL-Apo 10x/0.4 CS, Leica, Wetzlar, Germany). To visualize the position of the tetrode, we reconstructed the tetrode tracks together with neuron types of the central complex in 3D using the software Amira 5.3.3 (ThermoFisher, Germany). To visualize the tetrode positions from different experiments, we afterwards registered the tetrode position into the monarch butterfly standard central complex (*7*). We used an affine (12-degrees of freedom), followed by an elastic registration to transfer the neuropils of the individual central complexes into

the corresponding neuropils of the standard central complex. The registration and deformation parameters were then applied to the tetrode reconstruction to visualize the tetrodes in one frame of reference.

Spike sorting and spike shape analysis

Recordings were spike sorted with the tetrode configuration implemented in Spike2 (version 9.00, Cambridge Electronic Devices, Cambridge, UK). We used four spike detection thresholds (two upper and two lower thresholds). The highest and lowest thresholds were set to avoid large voltage deflections deriving from movement or electric stimulation artifacts being misinterpreted as spikes. The time window for template detection was set to 1.6 ms. After spike-sorting, a principal component analysis (PCA) was used to evaluate and to redefine spike clusters, if necessary. Spike2 channels were exported as down-sampled Matlab files (3 kHz) and the remaining analysis was done with custom written scripts in MATLAB (Version R2019b, MathWorks, Natick, MA, USA). To analyze the spike shapes and to perform correlation analysis, the WaveMark channels containing the spike-waveforms were additionally exported as non-down-sampled Matlab files (30 kHz). To ensure that we recorded from the same neuron throughout the experiment, we compared the neuron-specific spike shapes across different recording periods. For each behavioral state e.g., *quiescent pre-flight, fixed-flight, steering-flight, quiescent post-flight*, the average spike shape was constructed by calculating and merging the mean spike shape from each recording electrode along the time axis. This resulted in a total time window of 6.4 ms (4 x 1.6 ms) or 232 points corresponding to a sampling rate of 30 kHz for each behavioral state. The average spike shape during pre-flight was compared to the average spike shapes measured during flight (e.g., *fixed flight*, *steering flight*), and after flight (*quiescent post-flight*). This resulted in at least two correlation coefficients per neuron. We used the lowest correlation coefficient of each neuron to compare it to a modelled distribution of correlation coefficients generated by the correlation between the neuron's spike shape during pre-flight and all spike shapes obtained within one set of experiments [150 neurons for the state-dependent change experiments (Fig. 1, S2); 272 neurons for the electric stimulation experiments (Fig. S8); 55 neurons for pharmacological experiments (Fig. 3); 47 neurons for the passive rotation experiments (Fig. 4,S10); 37 neurons for the experiment using two suns (Fig. 2)]. The correlation with a randomly selected spike shape was repeated in total 1,000,000 times to obtain the distribution of correlation coefficients for each neuron. Only neurons that exhibited a statistically higher neuron-specific correlation coefficient than the modelled correlation coefficients ($p < 0.05$) were used for further analysis. 561 neurons passed this criterion and had an average correlation coefficient of 0.94 ± 0.08 (mean ± SD).

Experiment testing state-dependent changes in the preferred firing direction

To examine the neural response to a green light spot during quiescence, a green light spot was moved 360° around the animal during recording while the butterfly was sitting on a platform (Compact Lab Jack, Inc, Newton, New Jersey, USA; *quiescent pre-flight*). The angular velocity of the sun stimulus was set to 60°/s which is commonly used to characterize compass neurons in restrained insects (*6, 44, 50*). The light spot was moved in clockwise and counterclockwise directions. While recording from the same neuron, the stimulus condition was repeated (360° movement of the sun stimulus around the butterfly) but this time while the animal performed a tethered flight in one locked direction (0°, the same heading direction as in quiescence, *fixed flight*). Afterwards, the position of the sun stimulus remained stationary at 0° while the tethered

flying butterfly was free to rotate around its yaw axis (*steering flight*). In some experiments (n = 63 neurons), the butterfly was allowed to sit on the platform again to measure the neural response after flight (*quiescent post-flight*). To generate circular plots (bin size = 10°) showing the spatial tuning of recorded neurons and to calculate the preferred firing directions and vector strengths of each neuron, the CircStat (*51*) and CircHist (*52*) toolboxes of MATLAB were used. The neural sensitivity for coding the angular position of the sun stimulus was examined by testing if the neural response showed a uniform distribution ($p < 0.05$, Rayleigh test). If this was the case in one of the conditions, the preferred firing direction and the vector strength of a neuron was calculated.

Experiments with the two-sun stimulus

For the experiments with the two suns, two equally bright (1.74×10^{13} photons/cm^2/s) green light spots were positioned 180° apart from each other (at 0° and 180° with respect to the initial orientation of the animal). The neural response was measured during *quiescence* (pre- and post-flight) while the two suns were moved clockwise and counterclockwise around the animal (angular velocity: 60°/s). Additionally, the neural response was measured while the tethered flying butterfly was able to steer in the presence of the two sun stimuli (*steering flight*). A weighted fit model was used to test if the neural response was described by a Gaussian (weight < 0.5; unimodal) or a sine-square function (weight > 0.5; bimodal) (*44*). 33 central-complex neurons were sensitive in each of the three tested conditions (*quiescent pre-flight, steering flight, quiescent post-flight*). The weights were statistically compared across the conditions according to a RM one-way ANOVA + Holm Sidák's multiple comparison test (GraphPad Prism 9, GraphPad Software, San Diego, CA, USA).

Pharmacological and electrical stimulation experiments

For the pharmacological and electrical stimulation experiments, we did not fix the tetrode's position with Kwik-Sil to ensure that we still had access to the brain during the entire experiment.

For the pharmacological experiments, 10-20 µL of 500 µM chlordimeform diluted in saline (an octopamine agonist) was topically applied onto the brain while performing neural recordings in quiescent animals. We decided for a relatively high concentration of chlordimeform because the body dimensions of the monarch butterfly are larger than that of flies (*25, 26*) and we had to ensure that enough chlordimeform diffused to the central complex (depth: 200-300µm). The neural sensitivity for coding the angular position of the light spot was measured before treatment and in 10-minute intervals from the onset of chlordimeform treatment. The stimulus was moved around the animal in the same way as described above for quiescence. The neurons were recorded for about 40-140 minutes (mean = 70 ± 29 minutes). The neural sensitivity to the stimulus was measured before treatment and compared with the last measurement. In addition to the pharmacological experiments, we also performed electrical stimulation experiments that allowed us to precisely control the timing of treatment and to test if changes in neural sensitivity were local and reversible. To do so, two stimulation copper wires (resistance: ~1 MΩ) were connected to the EIB-18 and were waxed to the tetrode. The voltage of the electrical stimulation on the two stimulation wires was controlled through an Arduino (MEGA 2560). Electrical stimulations were applied as pulses (1 ms) and repeated at 20 and 40 Hz and with an electric current of 0.5-5 µA. The neurons' (n = 271 neurons) sensitivity to encode the angular position of the sun stimulus was measured before, during, and after electrical stimulation. High voltage deflections representing

artifacts from electric stimulations could easily be distinguished from the relatively low amplitude spike signals. The most upper and lowest spike detection threshold were set, so that high voltage deflections were not considered as neural signals (see also: Spike sorting and Spike shape analysis). If the neural response exhibited a uniform distribution ($p < 0.05$, Rayleigh test) before, during or after stimulation the neuron was considered to be sensitive to the sun stimulus.

The influence of stimulus history and velocity on neural tuning

To test for the influence of stimulus history on neural tuning, the simulated sun was moved with a constant velocity of 60°/s in an unpredictable manner around a quiescent butterfly (*unpredictable stimulus history*). To test for changes in preferred firing directions associated with stimulus velocity, we also varied the velocity of the sun stimulus between 20-80°/s while it was moved in an unpredictable manner around the animal (*unpredictable stimulus velocity*; stimulus details are plotted in Fig. S5A). The preferred firing directions obtained in these experiments were compared to the neural response of a predictable moving sun stimulus (*quiescent*). At the end of each experiment, the preferred firing directions were also measured during flight (*steering flight*). The preferred firing directions in *quiescence* and during *steering flight* were compared with the preferred firing directions obtained in response to the unpredictably moving sun stimulus conditions ($n = 42$ neurons). A V-test (expected mean: 0°) was used to test if the change in preferred firing direction was similar between two conditions. If the V-test was significant ($p < 0.05$) this means that data were clustered around 0° implying that the preferred firing direction did not change between the tested conditions.

Testing for coding of turning behavior

To test whether the recorded central-complex neurons encoded flight turns, we selected the flight sections in which the animal's heading changed more than 9° from its actual heading direction. We set 9° as threshold for turns because the angular sensitivity of the optical encoder was 3° and deviations of ± 3° could represent variations in flight direction rather representing flight turns. We then examined the firing rate prior to and after the moment of turn during a one-second window (500 ms prior and 500 ms after a flight turn). The neural activity during the turn was normalized to the firing rate 500 ms prior to the turn and was compared to the firing rate of sections in which the animal flew straight. Neurons were categorized as coding for flight turns if (i) changes in the normalized neural activity during flight turns were higher/lower than the changes occurring during periods of no turns (Wilcoxon p-test < 0.05) or (ii) if changes in the normalized neural activity during time windows of flight turns fitted a Gaussian distribution (> 0.6). 12 of the 150 (8%) neurons passed both criteria and were defined as neurons coding for flight turns. Only 7 of these 12 neurons additionally encoded the angular position of the light spot during flight.

Passive rotation experiments

To test for the influence of idiothetic cues on neural tuning, we mounted a platform on a rotation stage (DT-50, PI miCos, Eschbach, Germany) at the center of the LED arena. The butterfly was then fixed on the platform and the animal was rotated around its yaw axis. The motions of the

rotation stage were controlled by a custom written script in MATLAB. The neural response was first measured during *quiescence* as described above. Then, the butterfly was rotated clockwise and counterclockwise at 60°/s (*quiescence rotation*). During *quiescence rotation*, the sun stimulus was presented at 0° (in front of the animal at the beginning of rotation). Afterwards, the butterfly was rotated in the same way, but in the absence of any visual cue (*darkness rotation*). At the end of the experiment, the butterfly was unrestrained, and the neural response was measured while the butterfly was allowed to fly (*steering flight*). The directedness of the neural response during *rotation* and *darkness rotation* was represented by calculating the vector strength of the neural response. The preferred firing direction of each neuron (n = 16) was calculated for each behavioral state (*rotation*, *darkness rotation*, *quiescence*, *steering flight*). Only neurons that encoded the angular position of the simulated sun in all conditions were considered. If the preferred firing directions were similar across conditions, then the changes in preferred firing directions were found to cluster around 0° (V-test). Alternatively, if the changes were not found to cluster around 0°, they were tested for a uniform distribution (Rayleigh test: $p > 0.05$).

To test how the neural tuning changes if the animal is engaged in flight but is passively turned (instead of performing controlled steering), we performed similar experiments with the rotation stage mounted above the tethered animal. The tethered animal was then connected to the rotation stage and was passively rotated around its yaw axis (*rotation fixed flight*) while experiencing the simulated sun at 0°. The neural response of the neurons was compared to the responses recorded during quiescent situation (*quiescent pre-flight*) and when the animal was allowed to fly in one heading direction (*fixed flight*) while the sun stimulus was moved around the animal (at a velocity of 60°/s). After flight, the neural response was remeasured during quiescence (*quiescent post-flight*). The preferred firing directions of 17 neurons that encoded the angular position of the sun stimulus in all behavioral states were calculated and compared with the preferred firing direction during *quiescence* (pre-flight).

Conflict experiments

To test the relevance of the sun-stimulus in different behavioral states, we performed the same experiments as described above (*rotation*, *steering flight*), with the exception that the position of the sun stimulus was switched to the opposite side of the arena (180°) after three clockwise and counterclockwise rotations (*rotation*) or after 2 minutes of flight (*steering flight*). Afterwards, the experiment was repeated with the sun stimulus located at 180° relative to its original position. The change of the preferred firing direction was compared between the two conditions. If the preferred firing direction changed by 180° (V-test, expected direction:180°), then the preferred firing directions were dominated by the change in the simulated sun's position.

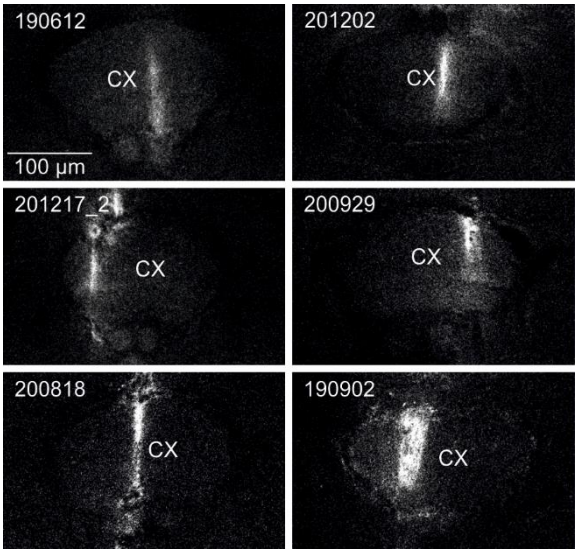

Fig. S1. Visualization of tetrode tracks from six experiments. Optical slices (z-slices) from the central body of the central complex showing the staining quality of tetrode tracks from some experiments. The tetrodes evidently run through the central body of the central complex (*CX*).

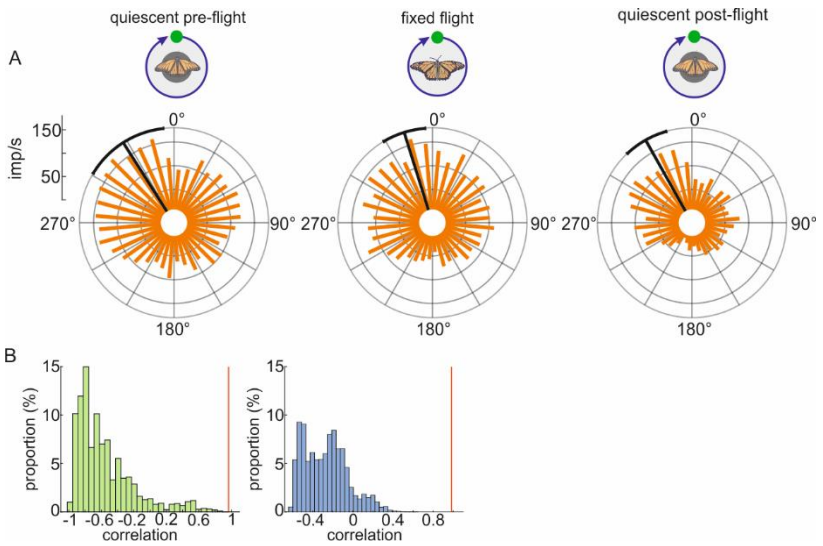

Fig. S2. Example neuron without state-dependent change in angular sensitivity, statistics for verifying spike-shape stability within two example neurons showing state-dependent changes. (A) Circular plots of firing rate at different solar azimuths in one example neuron showing no state-dependence across different behavioral states, i.e. *quiescent pre-flight (left), fixed flight (middle), quiescent post-flight (right)*. The animal faced 0° while the sun stimulus moved around. Black lines and sectors represent the preferred firing direction ± standard deviation (*SD*) of the neuron. (**B**) Distributions of correlation coefficients calculated by comparing the averaged spike shapes of the blue and green neuron from Fig. 1 with 1,000,000 randomly depicted averaged spike shapes of 150 recorded neurons. The correlation coefficient within the neuron is plotted as red vertical line.

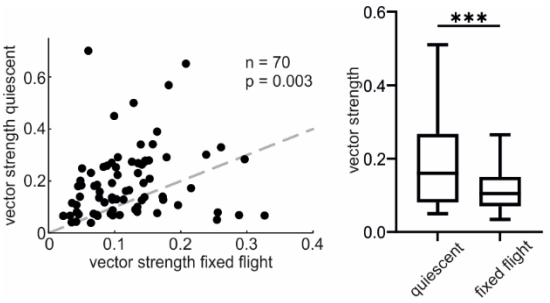

Fig. S3. Spatial tuning to the sun is broader during flight than during quiescence. (**A**) Scatter plot (*left*) and boxplots (*right*) show the vector strengths of the spatial tuning to the sun stimulus during *fixed flight* and quiescence. A decreased vector strength demonstrates that the solar azimuth is less precisely encoded during flight compared to during quiescence. ***: $p < 0.001$; Wilcoxon matched-pairs signed rank test.

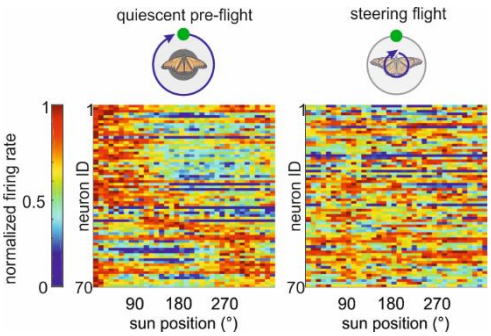

Fig. S4. Differences in neural tuning between *quiescent pre-flight* and *steering flight*. Neural tuning to the solar azimuth of all neurons showing angular sensitivity to the sun stimulus during *quiescent pre-flight* (*left*) and *steering flights* (*right*, n = 70 neurons). For reasons of comparison, neurons are ordered according to their preferred firing direction during *quiescent pre-flight*, along the y-axis.

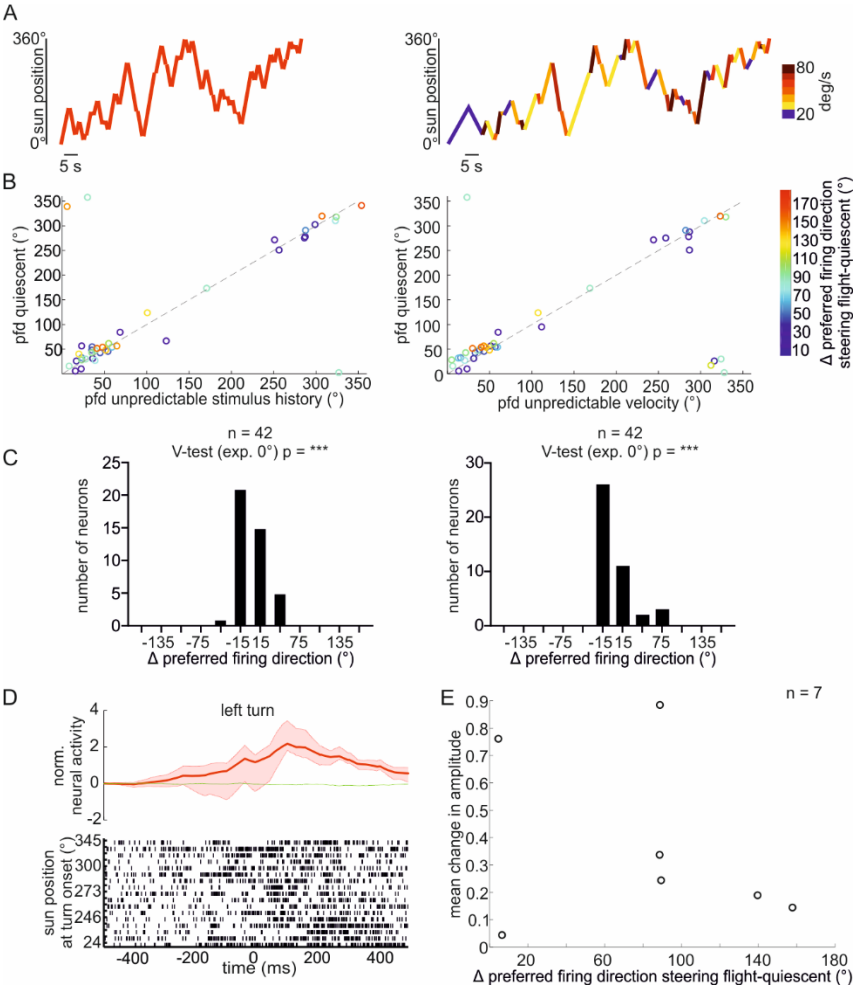

Fig. S5. Stimulus history, stimulus velocity, and encoding turning behavior do not account for changes in preferred firing directions (pfd) observed during steering flights. (**A**) (*Left*) Spatiotemporal dynamics of the stimulus that changes it's turning direction in an unpredictable manner (unpredictable stimulus history). (*Right*) Spatiotemporal dynamics of the stimulus that changes its turning direction *and* angular velocity (ranging from 20°-80°/s) in an unpredictable manner. (**B**) (*Left*) Scatter plot showing the relationship between the preferred firing direction during quiescence in which the stimulus was rotated with a constant velocity of 60°/s in full turns around the butterfly and the preferred firing direction calculated when the sun stimulus movement direction was unpredictable. Afterwards, the preferred firing direction was measured as the butterfly performed a steering flight. Color coded are the neural tuning shifts observed during steering flight. (*Right*) Same as in the left scatter plot but comparing the preferred firing directions between quiescent and unpredictable stimulus velocity. The preferred firing directions were similar between the compared stimulus conditions and neurons with large tuning shifts during steering flights (orange to red colored dots) do not show strong tuning shifts across variations in stimulus history or velocity. (**C**) Distribution of changes in preferred firing direction between quiescent and unpredictable stimulus history (*left*) and quiescent and unpredictable stimulus velocity (*right*). ***: $p < 0.001$; V-test (tested against 0°). (**D**) (*Top*) Sliding average shows the mean response (± interquartile range) to left turns for one example neuron. The averaged response at periods in which no turns occurred are plotted as green line. (*Bottom*) Raster plot of the example neuron in which the trials were ordered along the starting position of left turns. (**E**) Scatter plot of the response strength to flight turns, indicated by the mean change in response amplitude versus the shifts in preferred firing direction during steering flights. Only 7 out of the 150 recorded neurons responded to flight turns and also encoded the sun position during steering flight. No correlation between the neural tuning shifts during steering flights and the response strength to flight turns was observed which shows that the neural shifts cannot be explained by coding of turns.

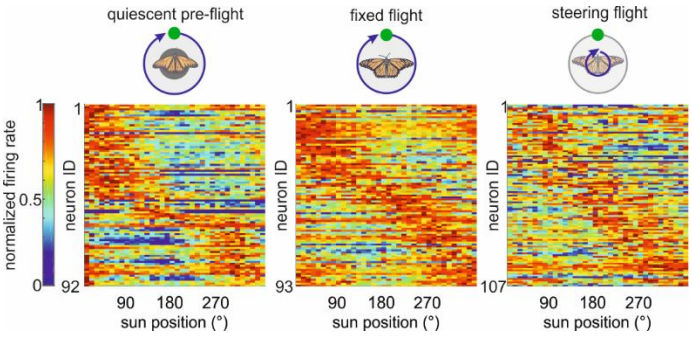

Fig. S6. Neural tuning and representation of solar azimuths within a neuronal population and at different behavioral states. Neural activity (*color coded*) is plotted against the sun position (*x-axis*) for each behavioral state [*quiescent pre-flight*, n = 92 neurons (*left*); *fixed flight*, n = 93 neurons (*middle*); *steering flight*, n = 107 (*right*)]. Since not every neuron showed angular sensitivity (Rayleigh test: $p < 0.05$) in all behavioral states, the number of neurons plotted in each heatmap are different.

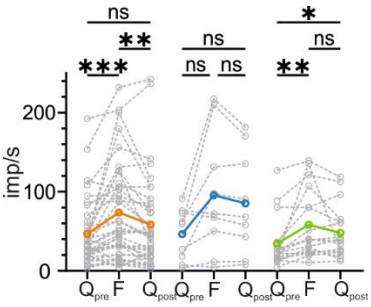

Fig. S7. State-dependent changes in neural activity. Changes in the firing rates across locomotion states, i.e. quiescence (pre: Q_{pre} and post: Q_{post}) and *fixed flights* for three different subpopulations of neurons. Orange group (n = 76): neurons being sensitive in each of the three locomotion states. Blue group (n = 16): neurons being sensitive only during quiesence. Green group (n = 50 neurons): neurons being sensitive only during fixed flights. Colored lines represent mean values. ***: $p < 0.001$; **: $p < 0.005$; *: $p < 0.05$ ns: $p > 0.05$ Friedman test.

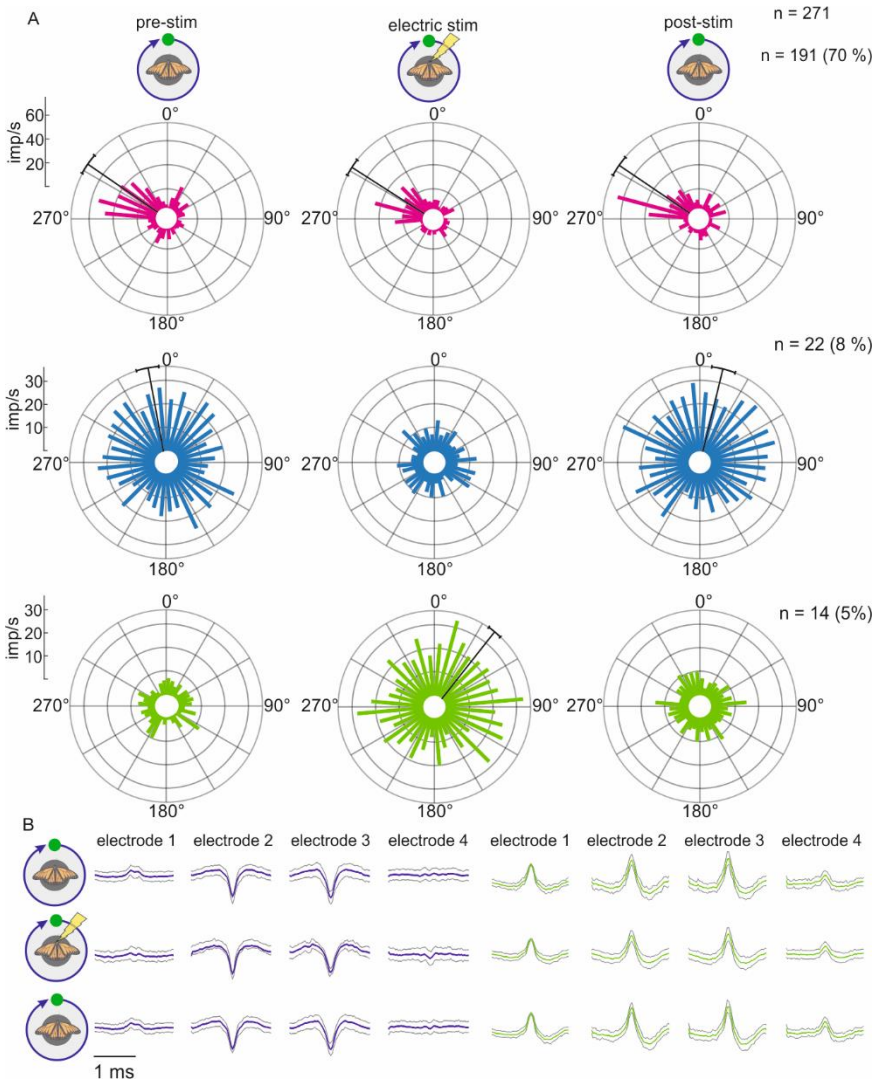

Fig. S8. Neural sensitivity to the sun stimulus could be modulated by electric stimulation. (**A**) Circular plots of three example neurons representing the effects of electrical stimulation on angular sensitivity. (*Top row*) One representative neuron of 191 neurons that encoded the sun position before, after and during electric stimulation on the tetrodes. (*Middle row*) One representative neuron of 22 that ceased encoding the sun as soon as an electric current was applied. (*Bottom row*) One representative neuron of 8 neurons that gained sensitivity for the sun as soon as an electric current was applied. (**B**) Averaged spike shapes (mean ± IQR) of the example blue and green neuron demonstrating highly similar spike shapes across the conditions (*pre-stim*, *electric stim*, *post-stim*).

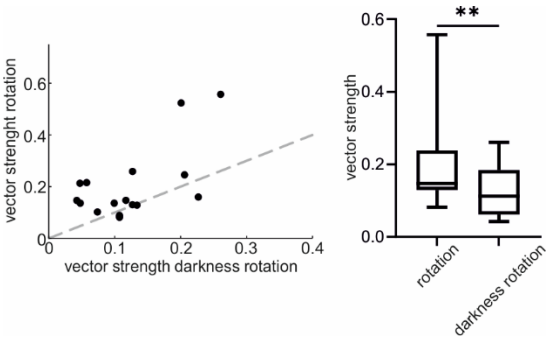

Fig. S9. Spatial tuning of heading-direction cells is broader during passive rotations in darkness than in the presence of the sun stimulus. Scatter plot (*left*) and boxplots (*right*) show the decrease in vector strength of the spatial tuning to the sun stimulus during passive rotations in darkness than during passive rotations in the presence of the sun stimulus. **: $p < 0.005$; Wilcoxon matched-pairs signed rank test.

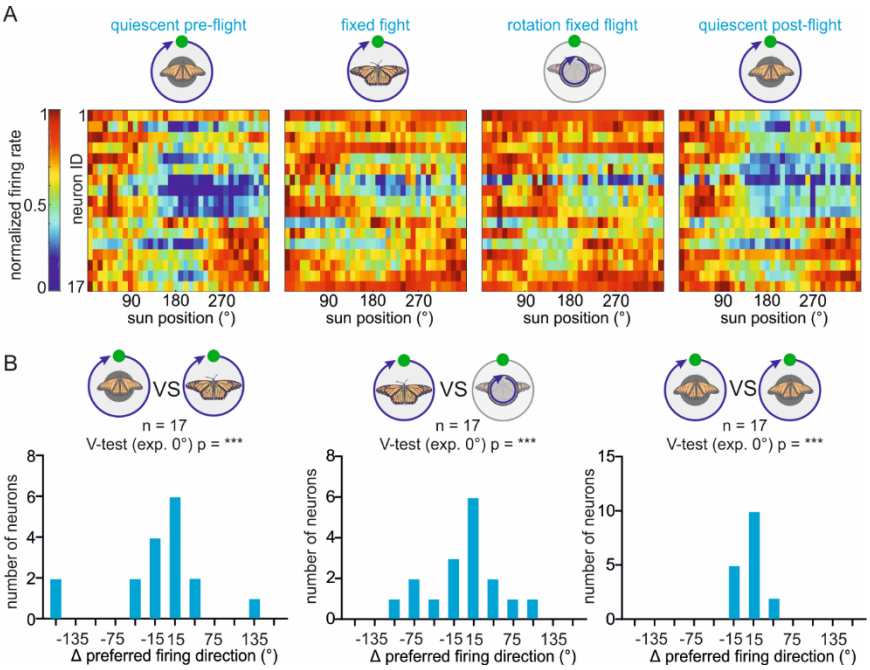

Fig. S10. Changes in flight direction without steering do not affect the preferred firing direction. (**A**) Neural activity of 17 neurons for each behavioral state i.e., *quiescent pre-flight*, *fixed flight*, *rotation fixed flight*, and *quiescent post-flight* is plotted against the sun position. Passive rotation during flight was measured by mounting the tethered butterfly dorsally on a rotation stage that allowed the butterfly to fly but not steer. (**B**) Changes in preferred fight direction between *quiescent pre-flight* and *fixed flight* (*left*), *quiescent pre-flight* and *rotation fixed flight* (*middle*), and *quiescent pre-flight* and *quiescent post-flight* (right). ***: $p < 0.001$; V-test (tested against 0°).

Movie S1. Example recording from a quiescent butterfly that was stimulated with a sun stimulus moving along a 360° circular path around the animal.

Movie S2. Example recording from a *fixed flight* while the sun stimulus was moved along a 360° circular path around the animal.

Movie S3. Example recording from a *steering flight* in which the flying butterfly was allowed to steer relative to a static sun stimulus.

Movie S4. Example recording from a quiescent butterfly that was stimulated with a sun stimulus moving with a constant angular velocity (60°/sec) in unpredictable directions along a 360° circular path around the animal.

Movie S5. Example recording from a quiescent butterfly that was stimulated with a sun stimulus moving with a varying angular velocity (20-80°/sec) in unpredictable directions along a 360° circular path around the animal.

Movie S6. Example recording from a quiescent butterfly that was rotated in presence of a sun stimulus (*left*) and in darkness (*right*).

Movie S7. Example recording from a fixed flying butterfly that was rotated by a dorsal rotation stage while a static sun stimulus was presented.